Research Article | Vol. 11, No. 1 / 1 January 2021 / Optical Materials Express 142
Optical Materials EXPRESS

Extruded suspended core fibers from lanthanum-aluminum-silicate glass

Doris Litzkendorf,[1,*] Anne Matthes,[1] Anka Schwuchow,[1] Jan Dellith,[1] Katrin Wondraczek,[1] and Heike Ebendorff-Heidepriem[2]

[1]Leibniz Institute of Photonic Technology (Leibniz-IPHT), Albert-Einstein-Str. 9, 07745 Jena, Germany
[2]Institue of Photonics and Advanced Sensing and School of Chemistry and Physics, The University of Adelaide, SA 5005, Australia
[*]doris.litzkendorf@leibniz-ipht.de

Abstract: We report the use of the extrusion technique at highest temperatures to date (975 °C - 1000 °C) for the fabrication of suspended core fibers (SCFs) from glass with molar composition 65 SiO_2-20 Al_2O_3-15 La_2O_3 (SAL65). Through adjusting die design and fabrication conditions, extruded preforms for fibers with two different core sizes (1.2 µm and 3.1 µm) were successfully produced. Cross-sectional microstructure and material loss of these fibers highlight the potential of the extrusion technique for fabrication of microstructured optical fibers from glasses with high softening temperature and thus high thermal and mechanical stability.

1. Introduction

Extrusion of a material at elevated temperature through a die or nozzle has been demonstrated to be a powerful technique to make optical fiber preforms from materials with low softening temperatures such as soft glasses and polymers. In this technique, bulk billets are heated up to a temperature where the material is sufficiently soft to be forced through a die structure by a ram to form an extrudate, which has a transverse profile with millimeter-scale features that is determined by the die exit geometry [1,2]. Key advantages are versatility in glass composition and a virtually unlimited flexibility in size, shape and arrangement of holes and multimaterials that can be achieved in a preform [2]. Therefore, a large range of fibers made from extruded preforms using a diverse variety of soft glass and polymer materials have been demonstrated to date [3–26]. Extrusion also enables long preform lengths, only limited by the billet volume that can be provided. Furthermore, extruded preforms exhibit an excellent surface finish due to the fire-polishing affected during cooling of the extruded glass in contact-less free space (i.e. without being in contact with a liquid or solid) [3,5].

In general, extrusion of glass can be conducted at temperatures anywhere between the deformation temperature (viscosity ~ 10^{11} dPa·s) and the softening temperature (viscosity 10^7 dPa·s) of the glass. The only premise is the absence of any degradation e.g. crystallization, phase separation, evaporation in this thermal regime over the extrusion time frame which can last from a few hours up to a day. To date, extrusion of optical fiber preforms has been limited to glass materials having a softening temperature of < 700 °C. The main reason is the availability of a suitable extrusion die material that can withstand higher temperatures whilst allowing continuous glass flow. The most widely used extrusion die material is stainless steel, which has been used successfully up to 650 °C [1].

Expanding extrusion to glass materials with higher softening temperatures allows utilization of the structure versatility of extrusion to such glasses, promising enhanced diversity in fiber

#409422 https://doi.org/10.1364/OME.409422
Journal © 2021 Received 3 Sep 2020; revised 5 Nov 2020; accepted 7 Nov 2020; published 16 Dec 2020

Optical Materials EXPRESS

design and properties. This motivated us to explore extrusion of silicate glass of the system SiO_2-Al_2O_3-La_2O_3 (SAL) with significantly higher softening temperature (> 900 °C) compared to soft glasses (< 700 °C). This aluminosilicate glass system represents an archetype group of glasses which combines many of the advantages of vitreous silica with the compositional flexibility of silicates, whereby alumina may act as network former or modifier, controlled by the type and concentration of a tertiary compound. While the classical alkaline earth aluminosilicates are receiving significant attention, for example for specialty consumer applications (related to their specific mechanical properties [27]), replacing the alkaline earth component by a rare earth component provides a further tool for notably enhancing the structural packing and bond energy densities. Furthermore, making use of the alumina avoidance rule, topochemical heterogeneity can be finely tailored which might be beneficial for further doping with optically active species [28].

SAL glasses offer further unique combinations of properties ranging between those of silica on one side and of soft and borosilicate glasses on the other side, i.e. thermal properties (transition temperature, thermal expansion) [29,30], mechanical properties (hardness and elastic modulus) [31,32], chemical durability [33], and optical properties (refractive index, nonlinearity) [34] as shown in Fig. 1(a). SAL glasses can be readily made using the melt-quench technology, which allows for high melting homogeneity, and thus high optical glass quality, as well as an easy volume up-scaling. Their high glass transition temperature combined with their low thermal expansion coefficient allows them to be combined with conventional silica fiber based components [35–39]. In addition, they provide high redox stability during thermal processing and large solubility capacity of various rare earth elements.

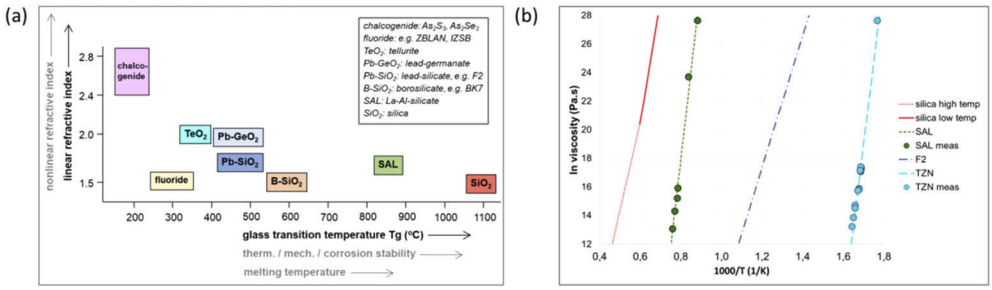

Fig. 1. (a) Schematic of the thermal and refractive index properties of a variety of glass families [47]. (b) temperature-viscosity-curves of selected glasses: silica, SAL65, lead-silicate F2 and tellurite glass TZN.

This unique combination of properties makes SAL glasses promising materials for different applications, such as high nonlinearity fibers for supercontinuum generation [35], optical fiber switching, Raman amplifiers/lasers, compact fiber lasers with high rare earth concentration [36,40] and bulk laser media [41,42]. SAL glass is also of interest for microstructured optical fibers. In particular, small-core suspended core fibers (SCFs) that are suited for nonlinearity or sensing applications. However, fabrication of SAL glass fibers has been limited to date to simple step-index solid structures [36].

In this paper, we report the fabrication of extruded SCFs with 1.2 µm – 3.1 µm core diameter from a SAL glass composition with a high SiO_2 content of 65 mol% (hereafter referred to as SAL65) and a high Al_2O_3 content of 20 mol% to ensure high solubility of La_2O_3 in the glass melt and hence avoid phase separation and crystallization. We selected the small-core SCF as fiber type since the sensitivity of the fiber loss on the core surface quality allows for evaluation of the impact of extrusion conditions on both volume and surface defect formation in the preform and fiber [11]. As the SAL65 glass has a high glass transition temperature of ~ 861 °C [36],

Optical Materials EXPRESS

the extrusion trials were undertaken at high temperatures of 975 °C - 1000 °C in an ambient atmosphere. To the best of our knowledge, this is the highest billet extrusion temperature range used to date for optical preform fabrication. Both suspended core preforms and jacket tubes were made successfully using the extrusion technique. SCFs were successfully drawn from the extruded preforms and tubes. These fibers show material loss comparable to SAL glass fibers made by other structuring methods, which demonstrates the suitability of the extrusion technique for glasses with high softening temperatures.

2. Experimental

2.1. Fabrication

We prepared two SAL65 glass SCFs with different core diameters of 1.2 µm and 3.1 µm respectively, to be able to draw conclusions on glass surface quality from the propagation loss in the fiber core. The fabrication of an SCF involved (1) fabrication of glass billets of ~ 30 mm outer diameter (OD) using the melt-quench technique, (2) extrusion of the billets into a structured preform of ~ 16 mm OD with suspended core geometry and a jacket tube of ~ 10 mm OD, (3) drawing the preform to a cane of ~ 1 mm - 2 mm (OD), (4) inserting the cane into the jacket tube and finally drawing this cane-in-tube assembly to an SCF with ~ 125 µm OD.

Billets: Based on the starting composition 65 mol% SiO_2-20 mol% Al_2O_3-15 mol% La_2O_3 (65-20-15), SAL65 glass blocks were fabricated in 500 g batches using a discontinuous two-step melting process in an ambient atmosphere to achieve glass blocks in a high optical quality without striaes. In the first step, the highly pure (3N - 5N) raw materials (SiO_2, $Al(OH)_3$, La_2O_3) were pre-melted in a covered platinum crucible at 1400 °C - 1650 °C for 8 hours, and the liquid melt was quenched in water to obtain glass particles. We used ultra-pure water (zero water) to avoid contamination during quenching. In the second step, the glass particles were re-melted in a platinum crucible with stirrer at 1650 °C for 8 hours. The melt was cast into a stainless steel mold to produce a homogeneous glass block ($30 \times 30 \times 100$ mm^3), which was slowly cooled to room temperature at 100 K/h [36]. The thus prepared SAL65 blocks were ground and polished into billets of 30 mm diameter and 40 mm - 70 mm length for the extrusion experiments.

Preforms and tubes: A customized extrusion machine, operated in an ambient atmosphere, was used for the extrusion trials [1]. Note that an ambient atmosphere was found to be suitable for all oxide-based soft glasses extruded to date through stainless steel dies at temperatures < 600 °C. For lead-silicate glasses, this was demonstrated by the result that the propagation loss of the light guided in small-core SCFs drawn from preforms extruded in an ambient atmosphere was as low as the material loss [6]. As the hitherto widely used die material stainless steel does not have sufficient oxidation resistance and mechanical strength at ~ 1000 °C [43], we evaluated a range of commercially available metal alloys for their properties at elevated temperatures up to 1100 °C. The alloy Nicrofer 6023H (NiCr-alloy with additions of Al and Ti) was found to have outstanding corrosion resistance and good mechanical strength up to 1200 °C in air [44], making it a suitable die material for SAL glass extrusion in an ambient atmosphere. Therefore, the extrusion dies and associated parts were made from this alloy. For the extrusion of the two preforms with different core sizes, we used die designs with the same diameter of 15.6 mm for the die exit that formed the preform OD, but with different diameters of 1.5 mm (Trial #1) and 3 mm (Trial #2) for the central orifice that formed the suspended core in the preform. The assembly of SAL65 glass billet and extrusion die was heated up to 975 °C - 1000 °C, at which the glass had a viscosity of 10^8 - 10^{10} dPa·s and therefore was sufficiently soft to be forced through the die at a constant ram speed of 0.2 mm/min. Depending on the length of the billets, this ram speed resulted in an extrusion time of 4 - 7 hours. When the glass started to emerge from the die exit, the glass flow entered a quasi steady-state regime, where the extrusion force remained approximately constant over time. The force in the quasi steady-state regime was used to determine the glass viscosity.

Optical Materials EXPRESS

Fibers: For the cane drawing step, both extruded preforms were sealed at the top end to achieve self-pressurization [45,46]. To realize the two different fiber core sizes during the fiber drawing step, two different concepts of pressurization of the canes were employed: self-pressurization for Cane #1 (smaller core) by sealing the top end of the cane, and active pressurization (3 kPa) with helium gas flow for Cane #2 (larger core). Each of the cane-in-tube assemblies was drawn to a SCF with outer diameter of 125 µm and a protective single layer acrylate coating (DSM 3471-3-14; refractive index of 1.51).

The preform and tube extrusion as well as cane and fiber drawing parameters used to fabricate the two differently core-sized SCFs, such as temperature, extrusion force, preform feed rate, drawing speed, pressure conditions, are summarized in Table 1.

Table 1. Experimental conditions for extrusion of preforms and tubes, and for drawing of canes and fibers for the two trials.

Trial	Type	Temperature (°C)	Ram or Feed speed (mm/min)	Draw Speed (m/min)	Extrusion Force (kN)	Preform or Cane Pressure during Drawing	Atmosphere
#1	tube	975	0.2		1.0		ambient atmosphere
	preform	1000	0.2		2.9		ambient atmosphere
	preform cane	1300	2.0	0.50		self-pressurization	helium
	fiber	1310	1.5	6.0		self-pressurization	helium
#2	tube	980	0.2		1.2		ambient atmosphere
	preform	990	0.2		5.0		ambient atmosphere
	preform cane	1310	4.1	0.24		self-pressurization	helium
	fiber	1330	1.4	10.5		3 kPa	helium

2.2. Characterization

The polished SAL65 billets were inspected visually for glass homogeneity (striae, bubbles, and inclusions). Thermal properties, such as the glass transition temperature (T_g), dilatometric softening point (T_s), and thermal expansion coefficient (α @ 300 °C - 600 °C), were measured with a vertical dilatometer (LINSEIS L75V) on SAL65 glass bars ($4 \times 4 \times 20$ mm^3) using a heating rate of about 5 K/min. The refractive index n was measured at a wavelength of 633 nm using a prism coupler (Model 2010, Metricon Co., Pennington, NJ, USA) with an accuracy of about 10^{-3}. The SAL65 glass composition was determined by quantitative electron probe microanalysis (EPMA) using energy and wavelength dispersive X-ray analysis (EDX, WDX, JEOL JXA-8800L). The molar fractions were determined within an accuracy of less than ± 5% relative to the expected glass composition.

To identify the presence of any defects and crystalline phases in the glass billets, preforms, canes, fibers and heat treated glass cubes ($4 \times 4 \times 4$ mm^3), they were inspected with optical microscope, scanning electron microscope (SEM), EPMA and X-ray diffraction (XRD, Panalytical X'Pert Pro).

The dimensions of preforms, tubes, canes and fibers (outer, inner and core diameters; strut width and wall thicknesses) were measured using cross-sectional images, taken with a digital camera for the preforms and tubes, an optical microscope for the canes and an SEM for the fibers.

Optical Materials EXPRESS

The propagation loss of the fibers was measured using the cut-back method, using a halogen lamp as white light source and a commercial spectrometer (SPECTRO 320D, Instrument Systems). Launching the light in different parts of the fiber, material loss and core loss can be distinguished. Since the SAL65 glass has a higher refractive index of 1.6 compared to the polymer coating with index of 1.5, the polymer coating acts as the cladding when light is launched into the whole fiber cross section. Thus, the light is guided in the outer solid region of the fiber cross section, and the corresponding loss will be dominated by the loss of the material itself. By contrast, if the light is launched and guided only in the small core of the fiber, the loss is dominated by core surface effects [11] such as scattering at surface crystals. This allows evaluation of the impact of extrusion and drawing process on core surface quality.

3. Results and discussion

3.1. Glass properties

The SAL65 glass shows a clearly higher transition temperature ($T_g \geq 860$ °C) and softening point ($T_s \geq 922$ °C) than the soft glasses (e.g. lead-silicate, tellurite, chalcogenide), which have softening points < 700 °C. The thermal expansion coefficient and refractive index of the SAL65 glass were measured to be $\alpha = 5.2 \times 10^{-6}$/K @ 300 °C - 600 °C and $n = 1.654$ @ 633 nm, respectively. Figure 1(a) illustrates that the SAL65 glass properties lie between that of soft glasses and that of silica.

All SAL65 glass billets were crystal-free and striae-free as verified by XRD measurements and visual inspection, respectively. Trial #1 billets were homogeneous, optical transparent and had no defects. Trial #2 billets showed some bubbles due to the use of a different platinum crucible, which had a rough surface caused by a special crucible manufacturing process. The glass compositions (mol%) of the billets measured by EPMA/WDX are close to that of the nominal SAL65 batch composition (65-20-15) but vary slightly for Trial #1 (65.7-19.6-14.8) and Trial #2 (64.4-20-15.7), with Trial #2 having slightly higher La_2O_3 content due to experimental uncertainty.

3.2. Glass flow behavior and viscosity

The viscosity η of the SAL65 glass at various extrusion temperatures was determined from the extrusion force and ram speed using Poiseuille flow theory as described for soft glasses in Ref. [1]. Briefly, using Poiseuille flow equation of complete sticking of the glass to the metal die during extrusion, the viscosity is calculated from the extrusion force in the quasi steady-state region, the fixed ram speed and a so-called die constant, which is determined by extruding glass with known temperature-viscosity-behavior. The experimental data from preform extrusions are shown in Fig. 1(b). The data can be well fitted with an Arrhenius equation of $\ln \eta = a + \frac{b}{T}$, where T is the absolute temperature in K, and a and b are fitting parameters. For comparison, we also show the data measured for in-house made tellurite glass with molar composition 75 TeO_2-15 ZnO-10 Na_2O (TZN) using the same method as for the SAL65 glass. Furthermore, we show the Arrhenius temperature-viscosity curves for lead-silicate glass (F2 from Schott Co.) and silica glass. For the lead-silicate glass, the Arrhenius parameters calculated from known viscosity data were verified using the extrusion method as described in detail in [1]. For silica, the published Arrhenius parameters were used from Ref. [48]. From the Arrhenius parameter b, the activation energy E_A was calculated ($b = E_A/R$, where R is the molar universal gas constant). SAL65 glass has high activation energy (1030 ± 50 kJ/mol) comparable to that of TZN tellurite glass (980 ± 40 kJ/mol), whereas lead-silicate glass (384 kJ/mol) and fused silica (515 kJ/mol in the high temperature range) have considerably lower activation energies.

Optical Materials EXPRESS

3.3. Geometrical dimensions of preforms, canes and fibers

Exemplary cross-sectional images of extruded preforms, tubes, and drawn canes and fibers are shown in Fig. 2, and their geometrical dimensions are listed in Table 2. The size of the extruded preforms and tubes along their lengths relative to the die exit is determined by die swell due to change in flow profile and by gravitational pull for the soft glass emerging from the die exit [3]. The combined effect of these factors led to a slightly larger diameter at the start of extrusion, followed by a taper of ≤ 2% OD variation relative to preform length. Note that such small taper can be readily compensated during drawing by adjusting the draw speed to achieve a constant cane or fiber OD. Table 2 shows the median OD for the extruded preforms and tubes.

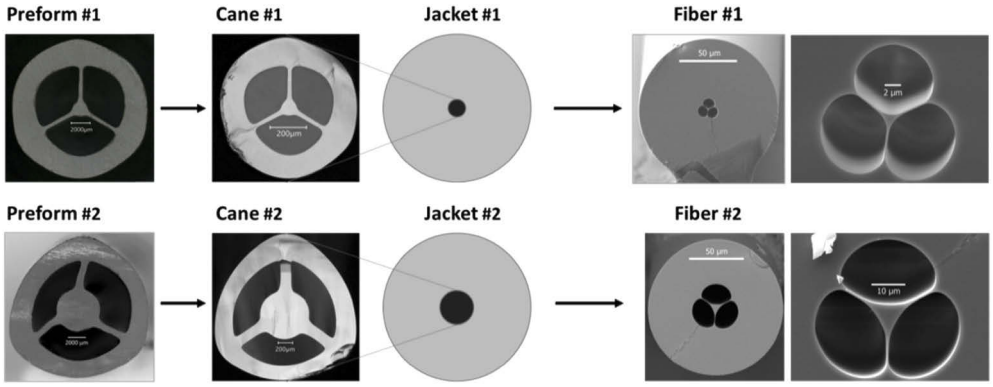

Fig. 2. Cross-sectional images of preforms, canes and fibers for the two trials.

Table 2. Cross-sectional dimensions (OD, core diameter, strut width) and dimension ratios for die, preform, cane, cane-in-tube assembly and fiber for the fabrication of Trials #1 and #2.

Trial	Type	Unit	OD[a]	Core	Strut	Core/OD (%)	Strut/OD (%)	Core/OD for[b]	Strut/OD for[b]
#1	die	mm	15.6	1.5	0.6	10	3.8		
	preform	mm	13.9	1.7	0.5	11	3.2	1.1	0.8
	cane	µm	762	86	23	11	3.0	1.0	0.9
	cane-in-tube	µm	9,000	86	23	1.0	0.3		
	fiber	µm	125	1.2	0.2	1.0	0.2	1.0	0.6
#2	die	mm	15.6	3.0	0.6	19	3.8		
	preform	mm	14.5	4.8	0.7	31	4.5	1.6	1.2
	cane	µm	2,125	679	146	32	6.9	1.0	1.5
	cane-in-tube	µm	10,600	679	146	6.3	1.4		
	fiber	µm	125	3.1	0.6	2.5	0.5	0.4	0.4

[a]OD of die exit and median OD of preforms and tubes with a taper of up to 2% along the length.
[b]Ratios preform/die, cane/preform and fiber/cane-in-tube.

For Trial #1, the preform was extruded using a die design that has been widely employed for soft glass to fabricate extruded SCFs [9,11–13,16]. As for soft glasses, the balanced flow in the die resulted in a SAL65 glass preform core size close to the target diameter of 1.5 mm (Table 2). Self-pressurization of the preform during cane drawing and of the cane during fiber drawing maintained the relative core and strut size (core/OD and strut/OD), leading ultimately to the target core diameter of ~ 1 µm for Fiber #1.

Optical Materials EXPRESS

For Trial #2, the increased flow in the core region (relative to the die of Trial #1) led to unbalanced flow between core and outer region in the die, causing a ~ 1.5 times larger core diameter of 4.8 mm relative to the target core diameter of 3.0 mm (Table 2). Self-pressurization of the Preform #2 maintained the relative core size, i.e. the cane core was also 1.5 times larger compared to the target design. To counterbalance this core size increase, the Cane #2 was actively pressurized with 3 kPa (helium gas). This resulted in a significant decrease in relative core and strut size of the Fiber #2 compared to the corresponding cane-in-tube assembly (Table 2), which enabled achieving the target core diameter of ~ 3 µm.

3.4. Surface defects of preforms, canes and fibers

A few millimeter-scale black inclusions were observed in the glass section from the beginning of extrusion for the preforms but not for the tubes. The black inclusions are attributed to metal oxide particles from the die. During heating up, when the die is not filled with glass, the metal surface becomes oxidized. Any small parts protruding from a die surface as a consequence of the die machining can be readily dislodged at elevated temperature due to the weakening of the material by the oxidation. Therefore, the glass flowing into the die at the beginning of extrusion can dislodge such metal oxide particles and embed them in the extruded glass. The glass bonds tightly to the oxidized metal surface of the die, as indicated by the glass flow within the die following Poiseuille flow behavior with zero slip coefficient at the glass/die interface [1]. Use of low extrusion speed as in this work ensures that this bonded layer is not disrupted. As a result, after the initial filling of the die with glass, any subsequent glass flows over this bonded glass layer, which prevents any further contamination from the die once any protruding parts from the die surface have been dislodged at the beginning of the extrusion process. The observation of the black inclusion only for the preforms is attributed to localized high shear rate within the finely structured dies used for the preform extrusion. The high shear rate facilitates shedding of protruding metal oxide particles from the die. As the preform sections with the black inclusions were limited to short length at the beginning of extrusion, they could be readily cut off so that the preform pieces used for cane and fiber drawing did not contain these defects.

Both the extruded preforms and the extruded tubes of Trials #1 and #2 showed micro-size isolated particles on their internal surfaces under an optical microscope. In contrast to the black inclusions, these micro-scale defects were observed over the whole length of the preforms and tubes. Similar isolated particles were also observed on the internal surface of the canes that were drawn from these preforms. To investigate these particles, SEM images were taken from the internal surface of the preforms and canes (Fig. 3). The images show micro-size bright spots for both the preforms and canes. The jagged edges of these surface spots suggest that they are crystals, which was verified by XRD measurements as described below. Cane #1 shows small crystals with similar appearance and size of a few micrometers relative to the crystals in the corresponding Preform #1. In addition, Cane #1 shows typical “crystal tracks” formed when drawing a preform with crystals. The similar crystal appearance and size for cane and preform as well as the presence of “crystal tracks” for the cane indicate absence of crystal growth during cane drawing. This favorable observation is attributed to the much shorter process time during cane drawing with about tens of minutes as compared to the more than 10 times longer extrusion time despite higher drawing process temperature. Similar to Trial #1, the few small crystals seen in the Cane #2 image (top left part of the image) have similar size of sub-micrometer as for the corresponding Preform #2. This result confirms the favorable observation of absence of crystal growth also for Cane #2. Note that the big feature in the middle of the SEM image of Cane #2 is attributed to an agglomeration of small crystals, which is consistent with the uneven distribution of crystals, including areas of high crystal density, in the corresponding Preform #2.

In addition to the surface crystals, the SEM images of the preforms show dark lines, which are attributed to scratches and other surface features indicating enhanced surface roughness.

Optical Materials EXPRESS

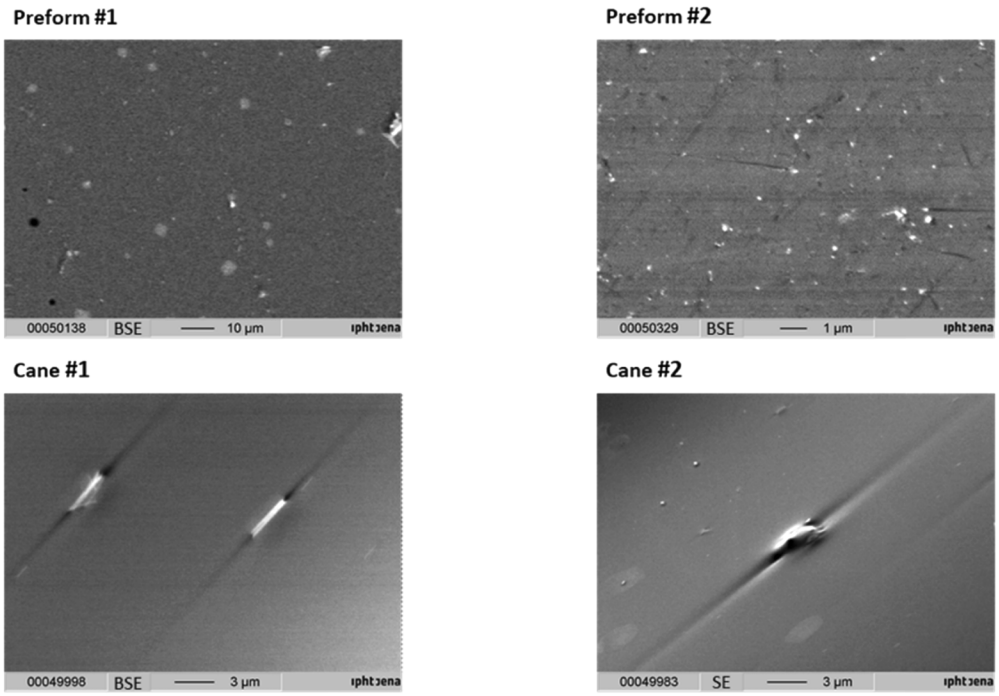

Fig. 3. SEM/BSE images of the extruded preform and drawn cane surfaces for the two trials.

Comparing these surface features of the extruded SAL65 glass with extruded lead silicate glass [5], we conclude that these surface features are caused from the flow of glass over the die surface with relatively high surface roughness. The fire-polishing effect during drawing of a preform into a cane leads to a smoothening of the surface as illustrated in the SEM images in Fig. 3.

The bright contrast of the surface crystals relative to the surrounding glass matrix in the back-scattered electron (BSE) micrographs (Fig. 3) indicates a higher concentration of heavy elements, e.g. lanthanum, in the crystals compared to the neighboring base glass material. This was confirmed by EDX proving the presence of lanthanum-rich crystals on the surfaces.

In order to investigate the SAL65 glass stability under extrusion conditions as well as any impact of temperature and time on surface quality, various cleaning processes and heat treatment experiments on SAL65 cubes of 4 mm length were carried out. In order to simulate the extrusion conditions as realistically as possible, the maximum temperature ranged from 980 °C - 1100 °C with holding periods of 4 - 7 hours under an ambient atmosphere. Before any heat treatment, the glass cubes were ultrasonically cleaned with various cleaning agents (isopropanol, methanol, 2% Hellmanex II-solution). Micro-size crystals appeared on the surface of SAL65 cubes at a temperature of 1050 °C, as shown in Fig. 4. This temperature is about ~ 50 K higher than the SAL65 extrusion temperatures (975 °C - 1000 °C). The higher temperature needed to form crystals on the cubes compared to the somewhat lower temperature at which crystals were formed during extrusion is attributed to the lack of shear stress in case of the cubes compared to the extruded material. The crystal size and number increase as the heating temperature rises irrespective of the cleaning procedure, indicating that cleaning does not cause any surface effects.

SEM imaging revealed that the annealed glass cubes showed crystallites on the sample surface but no crystallization within the sample volume (Fig. 5(a)). This behavior coincides with the observation on extruded preforms and tubes, where crystals were only found on the internal

Optical Materials EXPRESS

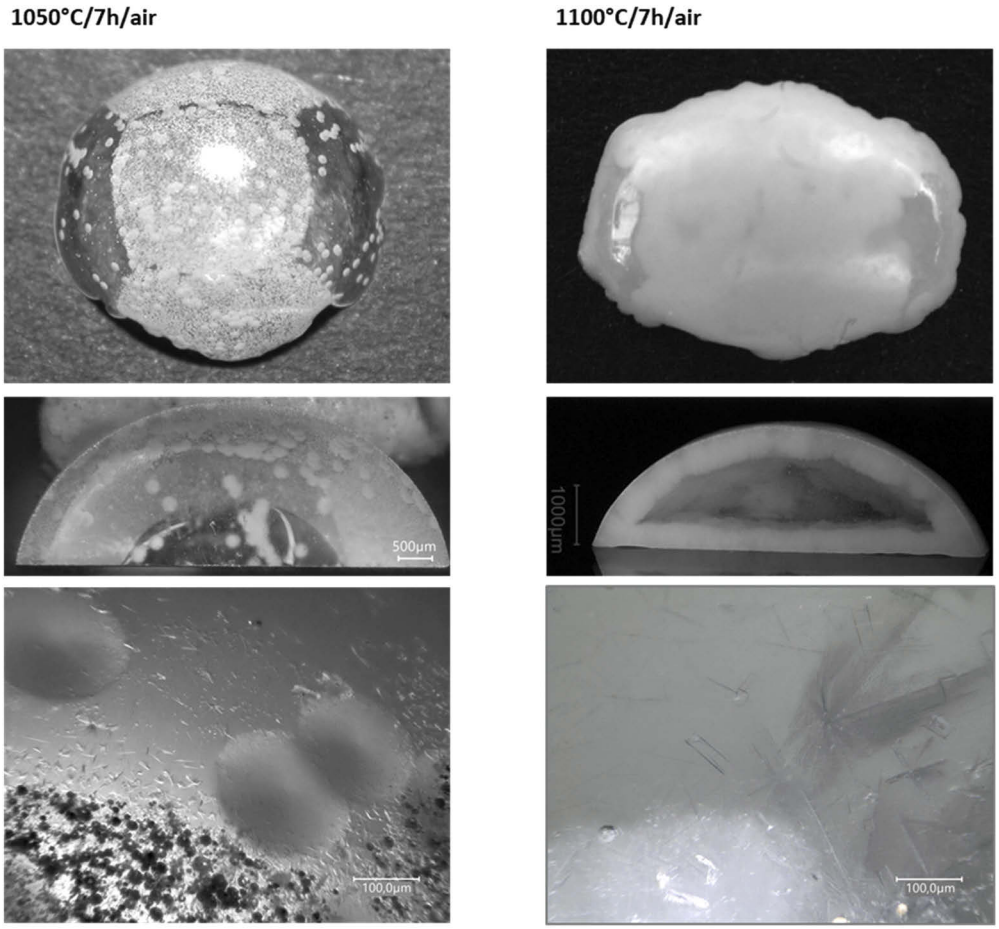

Fig. 4. Photo and optical microscope images of the surface of glass cubes heat treated at 1050 °C and 1100 °C for 7 h in an ambient atmosphere. For temperatures at 980 °C and 1025 °C no crystals were observed, images are not shown.

surfaces. The thickness of the crystallized surface layer of the cubes was measured to be in the range of 200 µm – 600 µm depending on the heating temperature. SEM imaging also indicated that the crystalline surface layer has different structural features including a needle-shaped network and isolated, bright appearing grain-like structures which is demonstrated in Figs. 5(a) and 5(b) taken at different magnifications.

One of the probable crystalline structures formed by the heat treatment could be lanthanum disilicate $La_2Si_2O_7$ with molar composition 66.7 SiO_2-33.3 La_2O_3. EDX spot analysis of the bright, white appearing grain-like structures (Fig. 5(b)) identified a phase with molar composition 69.5 SiO_2-0.7 Al_2O_3-29.7 La_2O_3, which is close to the above mentioned lanthanum disilicate. The small aluminum content is obviously a consequence of the simultaneously excited aluminum containing glass phase. The bright contrast of the grain-like structure is a consequence of the increased lanthanum content relative to the needle-network structure. The composition of the SiO_2-Al_2O_3-La_2O_3 glass phase in the sample volume measured by EPMA/EDX is 66.8-20.4-12.8 mol%, which is close to the glass batch composition. A comparison of two EDX spectra of the bright crystalline phase on the sample surface and the non-crystalline phase in the sample volume is shown in Fig. 6. The region with the needle-shaped network of crystals has a comparable

Optical Materials EXPRESS

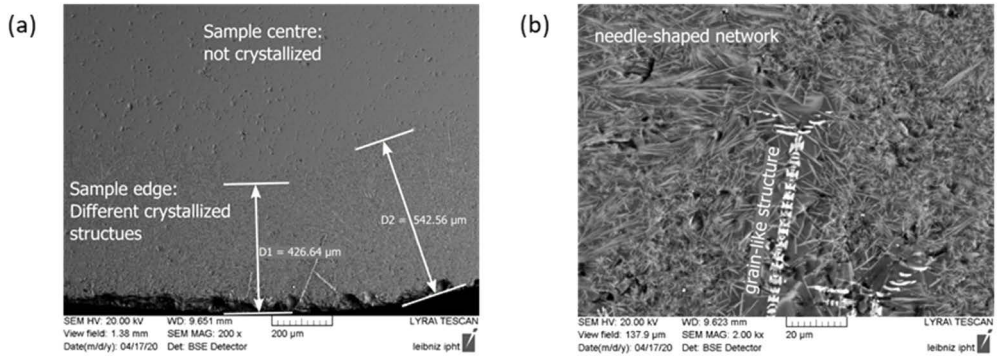

Fig. 5. Back-scattered electron micrograph (BSE) of glass cube heat treated at 1100 °C for 7 h in an ambient atmosphere. (a) Sample cross sectional view: crystallized region on sample surface but not in the sample volume visible. (b) Sample surface: different crystalline structures on the sample surface visible, needle-shaped network as well as bright appearing grain-like structures. Note, Figs. 5(a) and 5(b) have different magnifications.

composition as the homogeneous and crystal-free sample volume, indicating similar composition for these crystals and the glass.

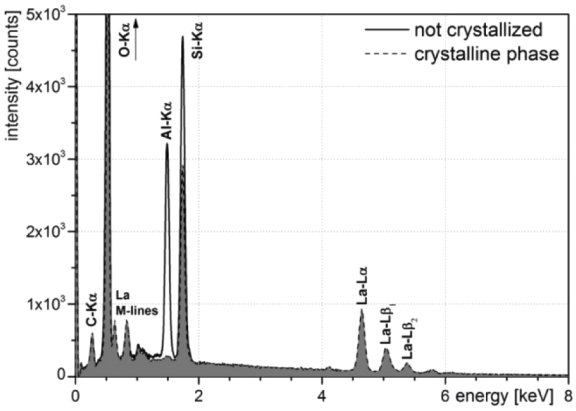

Fig. 6. Comparison of EDX spectra taken from the sample volume without any crystalline features (solid line) and the bright appearing, aluminum free structure in the crystallized surface region (dashed line).

XRD measurements revealed small crystalline peaks in addition to the broad amorphous glass hump. Figure 7 shows one XRD pattern (after subtraction of the broad glass hump) of SAL65 glass cube heat treated at 1100 °C for 7 h in an ambient atmosphere. The peaks are identified as lanthanum aluminum silicate $LaAlSiO_5$ (ICDD powder diffraction file 98-008-0753) and disilicate $La_2Si_2O_7$ (ICDD powder diffraction file 98-000-7071). The identified disilicate phase $La_2Si_2O_7$ agrees with the XRD studies to the crystallization behavior of SAL glasses by Sadiki *et al*. [49]. Based on the comparison of our results with that by Sadiki *et al*., we assign the isolated aluminum-free bright appearing grain-like crystals to $La_2Si_2O_7$ (identified via XRD and EDX). Based on the similar composition between needle-shaped crystals and glass, the needle-shaped crystals are assigned to the aluminum containing crystalline phase $LaAlSiO_5$ (identified via XRD). Quantitative phase analysis according to the Rietveld method shows that the two crystalline phases have proportions of approximately 75% $LaAlSiO_5$ and 25% $La_2Si_2O_7$.

Optical Materials EXPRESS

This result supports the assignment of the abundant network of needle-shape crystals and isolated, bright appearing grain-like crystals to $LaAlSiO_5$ and $La_2Si_2O_7$, respectively.

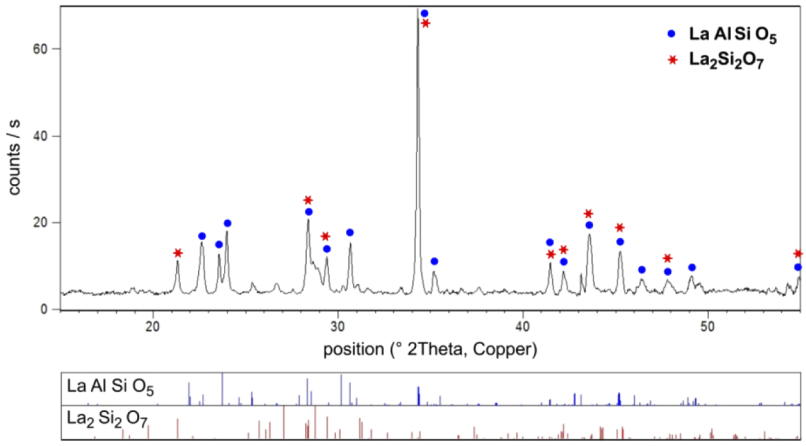

Fig. 7. XRD pattern of a glass cube heat treated at 1100 °C for 7 h in an ambient atmosphere (after subtraction of the amorphous glass hump).

The SEM, EDX and XRD investigations show that the isolated, grain-like $La_2Si_2O_7$ crystals on the surface of heat-treated SAL65 cubes have similar dimensions and lanthanum-rich composition as the isolated surface crystals on the extruded preforms and drawn canes, suggesting that the heat treatment during extrusion caused the crystallization. The lack of needle-shape network of $LaAlSiO_5$ crystals for the preforms and tubes indicates that these crystals are formed in detectable quantities only at higher temperature than the extrusion temperature.

The formation of crystals on the glass surface exposed to an ambient atmosphere suggests a crystallization mechanism similar to that identified for silica, where surface imperfections and water from the ambient atmosphere facilitate surface crystallization [50–52]. The surface imperfections induce heterogeneous nucleation, while the reaction of water molecules with the glass surface at elevated temperature results in a surface layer with lower viscosity compared to the glass volume, which accelerates crystal growth [50,51]. Under extrusion conditions, the high shear stress on the inner die walls that form the internal surfaces of the extruded preforms and tubes is likely to introduce surface imperfections, e.g. scratches from shear of the glass on the die wall, which facilitates heterogeneous nucleation, thereby reducing the onset temperature of surface crystallization compared to the glass cubes heated without shear stress. The water vapor in the ambient atmosphere used for extrusion is likely to enhance growth of the crystal seeds formed via heterogeneous nucleation on surface defects.

3.5. Fiber loss

The material and core loss spectra of both extruded SCFs (Trial #1 and #2) are shown in Fig. 8. For Trial #1 fiber, the material loss (measured on the whole fiber cross-section) is ~ 2 dB/m @ 1200 nm (Fig. 8(a)). This loss value is in the range of typical material losses of 0.5 - 10 dB/m for unstructured SAL glass fibers due to variations in contaminations from raw materials and crucibles [36]. The Trial #2 fiber has a higher material loss of ~ 5 dB/m @ 1200 nm and also a larger slope for the loss increasing towards shorter wavelengths. The higher loss correlates with the larger bubble content in the Trial #2 billets used for Trial #2 fiber fabrication. Both the increased slope and the overall loss increase over the whole wavelength range indicate the presence of both sub-micro-size bubbles causing Rayleigh scattering and larger size bubbles causing wavelength independent scattering, respectively [53].

Optical Materials EXPRESS

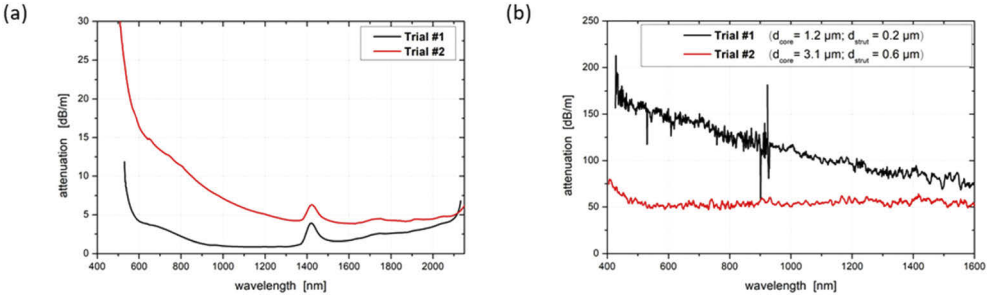

Fig. 8. Fiber loss spectra of the fibers of Trial #1and #2. (a) Light launched into the whole fiber cross section and (b) light launched into the core.

Both SCFs show core attenuation in the range of 50 - 90 dB/m @ 1200 nm (Fig. 8(b)). The core loss values are significantly higher than the material loss values. We attribute this difference mainly to light scattering caused by the surface crystals. As discussed in Section 3.4, extruded preforms and tubes as well as canes of Trials #1 and #2 showed surface crystals that remained during fiber drawing. The higher core loss for the Trial #1 fiber with a smaller core of ~ 1 µm is consistent with the statement of [11] that the effect of surface roughness on loss increases with decreasing core diameter d as $1/d^3$. This result suggests that the surface roughness due to the formation of surface crystals during extrusion dominates the core loss of the fabricated SCFs.

4. Summary and conclusions

SAL65 glass with high softening temperature > 900 °C was successfully extruded into structured preforms and tubes at high temperatures of 975 °C - 1000 °C. To the best of our knowledge, this is the highest temperature range used to date for extrusion of billets with optical quality. The SAL65 glass shows similar Poiseuille flow behavior during extrusion as soft glass. This allows the determination of the temperature-viscosity dependence of SAL65 glass according to the method used for soft glasses. The activation energy of viscous flow was calculated to be 1030 ± 50 kJ/mol. The extruded preforms and tubes were drawn to SCFs with two different core sizes of 1.2 µm and 3.1 µm, respectively. The successful fabrication of these fibers demonstrates the high potential of the extrusion technique for the manufacture of MOFs from glasses with high softening temperature and thus high thermal and mechanical stability.

The extruded preforms and tubes exhibit lanthanum-rich, micro-size crystals on their internal surfaces. Heat treatment of SAL65 glass cubes in an ambient atmosphere at temperatures above the extrusion temperature range revealed two crystalline phases on the glass surface, lanthanum aluminum silicate $LaAlSiO_5$ and disilicate $La_2Si_2O_7$. Compared to the heat treatment of the glass cubes without external force, the application of a force during extrusion led to the formation of surface crystals at lower temperature and only on internal glass surfaces. This behavior indicates that the high shear stress at the extrusion die inner walls induces the observed surface defects, which facilitate heterogeneous nucleation. The reaction of glass surface with water vapor from the ambient atmosphere used for the extrusion trials leads to a surface glass composition with reduced viscosity, which accelerates crystal growth.

The material loss of both extruded SCFs is < 5 dB/m @ 1200 nm, which is in the range of SAL glass fibers made via other methods. Due to surface crystals, the loss of the light guided in the small cores is with 50 - 90 dB/m @ 1200 nm one order of magnitude higher compared to the material loss. A promising route to avoid this surface crystallization is the prevention of the two effects facilitating heterogeneous nucleation. The effect of moisture can be mitigated by using dry inert atmosphere as demonstrated for annealing of silica glass [50]. The effect of

Optical Materials EXPRESS

surface roughness related defects on the extruded glass can be reduced by finishing the internal die surfaces upstream from the die exit over short length of 1 - 2 mm, which was shown for lead silicate glass to substantially improve the surface quality of the extruded glass [5].

This paper demonstrates that the advantage of the extrusion technology in terms of flexibility in size and shape of structures can also be utilized for SAL glass with high softening temperature. This offers the opportunity to produce SAL glass preforms and tubes in a large variety of geometrical dimensions by faster extrusion processing as compared to the limited geometrical structures possible with time consuming mechanical processing. Thus, the extrusion of SAL glass provides a large potential for the preparation of microstructured optical fibers, in particular for small core SCFs for high nonlinearity or sensing applications.

Funding

Thüringer Ministerium für Wirtschaft, Arbeit und Technologie (2012 FE 9063, 2012 VF 0020 (LASIL)); Bundesministerium für Bildung und Forschung (03WKCV01E (TOF)); Leibniz Association's Open Access Publishing Fund (Leibniz-Gemeinschaft); Government of South Australia (IRGP6).

Acknowledgments

The authors would like to thank P. Dittmann at Leibniz-IPHT for help in preparing glass melts, A. Dellith and M. Diegel at Leibniz-IPHT for SEM and XRD measurements, and A. Dowler at University of Adelaide for undertaking the extrusion trials. This work was performed, in part, at the Opto Fab node of the Australian National Fabrication Facility supported by the Commonwealth and SA State Government.

Disclosures

The authors declare no conflicts of interest.

References

1. H. Ebendorff-Heidepriem and T. M. Monro, "Analysis of glass flow during extrusion of optical fiber preforms," Opt. Mater. Express **2**(3), 304–320 (2012).
2. H. Ebendorff-Heidepriem and T. M. Monro, "Extrusion of complex preforms for microstructured optical fibers," Opt. Express **15**(23), 15086–15092 (2007).
3. C. A. G. Kalnins, K. J. Bachus, A. Gooley, and H. Ebendorff-Heidepriem, "High precision extrusion of glass tubes," Int. J. Appl. Glass Sci. **10**(2), 172–180 (2019).
4. G. Tsiminis, K. J. Rowland, E. P. Schartner, N. A. Spooner, T. M. Monro, and H. Ebendorff-Heidepriem, "Single-ring hollow core optical fibers made by glass billet extrusion for Raman sensing," Opt. Express **24**(6), 5911–5917 (2016).
5. H. Ebendorff-Heidepriem, J. Schuppich, A. Dowler, L. Lima-Marques, and T. M. Monro, "3D-printed extrusion dies: a versatile approach to optical material processing," Opt. Mater. Express **4**(8), 1494–1504 (2014).
6. H. Ebendorff-Heidepriem, Y. Li, and T. M. Monro, "Reduced loss in extruded soft glass microstructured fibres," Electron. Lett. **43**(24), 1343–1345 (2007).
7. C. A. G. Kalnins, N. A. Spooner, T. M. Monro, and H. Ebendorff-Heidepriem, "Surface Analysis and Treatment of Extruded Fluoride Phosphate Glass Preforms for Optical Fiber Fabrication," J. Am. Ceram. Soc. **99**(6), 1874–1877 (2016).
8. J. Bei, T. M. Monro, A. Hemming, and H. Ebendorff-Heidepriem, "Fabrication of extruded fluoroindate optical fibers," Opt. Mater. Express **3**(3), 318–328 (2013).
9. M. Oermann, H. Ebendorff-Heidepriem, D. J. Ottaway, D. G. Lancaster, P. Veitch, and T. M. Monro, "Extruded microstructured fiber lasers," IEEE Photonics Technol. Lett. **24**(7), 578–580 (2012).
10. H. Ebendorff-Heidepriem, T.-C. Foo, R. C. Moore, W. Zhang, Y. Li, T. M. Monro, A. Hemming, and D. G. Lancaster, "Fluoride glass microstructured optical fiber with large mode area and mid-infrared transmission," Opt. Lett. **33**(23), 2861–2863 (2008).
11. H. Ebendorff-Heidepriem, S. C. Warren-Smith, and T. M. Monro, "Suspended nanowires: fabrication, design and characterization of fibers with nanoscale cores," Opt. Express **17**(4), 2646–2657 (2009).
12. S. Afshar V, W. Q. Zhang, H. Ebendorff-Heidepriem, and T. M. Monro, "Small core optical waveguides are more nonlinear than expected: experimental confirmation," Opt. Lett. **34**(22), 3577–3579 (2009).

Optical Materials EXPRESS

13. H. T. Munasinghe, A. Winterstein-Beckmann, C. Schiele, D. Manzani, L. Wondraczek, S. Afshar V, T. M. Monro, and H. Ebendorff-Heidepriem, "Lead-germanate glasses and fibers; a practical alternative to tellurite for nonlinear fiber applications," Opt. Mater. Express **3**(9), 1488–1503 (2013).
14. S. C. Warren-Smith, A. Dowler, and H. Ebendorff-Heidepriem, "Soft-glass imaging microstructured optical fibers," Opt. Express **26**(26), 33604–33612 (2018).
15. W. Shengling, S. Fleming, B. T. Kuhlmey, H. Ebendorff-Heidepriem, and A. Stefani, "Effects of pressurization and surface tension on drawing Ge-Sb-Se chalcogenide glass suspended-core fiber," Opt. Mater. Express **9**(4), 1933–1944 (2019).
16. H. Ebendorff-Heidepriem, P. Petropoulos, S. Asimakis, V. Finazzi, R. C. Moore, K. Frampton, F. Koizumi, D. J. Richardson, and T. M. Monro, "Bismuth glass holey fibers with high nonlinearity," Opt. Express **12**(21), 5082–5087 (2004).
17. V. V. Kumar, A. K. George, J. C. Knight, and P. Russell, "Tellurite photonic crystal fiber," Opt. Express **11**(20), 2641–2645 (2003).
18. X. Feng, W. H. Loh, J. C. Flanagan, A. Camerlingo, S. Dasgupta, P. Petropoulos, P. Horak, K. E. Frampton, N. M. White, J. H. V. Price, H. N. Rutt, and D. J. Richardson, "Single-mode tellurite glass holey fiber with extremely large mode area for infrared nonlinear applications," Opt. Express **16**(18), 13651–13656 (2008).
19. K. Itoh, K. Miura, I. Masuda, M. Iwakura, and T. Yamashita, "Low-loss fluorozirco-aluminate glass fiber," J. Non-Cryst. Solids **167**(1-2), 112–116 (1994).
20. S. D. Savage, C. A. Miller, D. Furniss, and A. B. Seddon, "Extrusion of chalcogenide glass preforms and drawing to multimode optical fibers," J. Non-Cryst. Solids **354**(29), 3418–3427 (2008).
21. X. Feng, F. Poletti, A. Camerlingo, F. Parmigiani, P. Horak, P. Petropoulos, W. H. Loh, and D. J. Richardson, "Dispersion-shifted all-solid high index-contrast microstructured optical fiber for nonlinear applications at 1.55μm," Opt. Express **17**(22), 20249–20255 (2009).
22. Z. G. Lian, Q. Q. Li, D. Furniss, T. M. Benson, and A. B. Seddon, "Solid microstructured chalcogenide glass optical fibers for the near- and mid-infrared spectral regions," IEEE Photonics Technol. Lett. **21**(24), 1804–1806 (2009).
23. R. R. Gattass, D. Rhonehouse, D. Gibson, C. C. McClain, R. R. Thapa, V. Q. Nguyen, S. S. Bayya, R. J. Weiblen, C. R. Menyuk, L. B. Shaw, and J. S. Sanghera, "Infrared glass-based negative-curvature antiresonant fibers fabricated through extrusion," Opt. Express **24**(22), 25697–25703 (2016).
24. G. Tao, S. Shabahang, H. Ren, F. Khalilzadeh-Rezaie, R. E. Peale, Z. Yang, X. Wang, and A. F. Abouraddy, "Robust multimaterial tellurium-based chalcogenide glass fibers for mid-wave and long-wave infrared transmission," Opt. Lett. **39**(13), 4009–4011 (2014).
25. M. Zhu, X. Wang, Z. Pan, C. Cheng, Q. Zhu, C. Jiang, Q. Nie, P. Zhang, Y. Wu, S. Dai, T. Xu, G. Tao, and X. Zhang, "Fabrication of an IR hollow-core Bragg fiber based on chalcogenide glass extrusion," Appl. Phys. A **119**(2), 455–460 (2015).
26. T. M. Monro, Y. D. West, D. W. Hewak, N. G. R. Broderick, and D. J. Richardson, "Chalcogenide holey fibers," Electron. Lett. **36**(24), 1998–2000 (2000).
27. A. Pönitzsch, M. Nofz, L. Wondraczek, and J. Deubener, "Bulk elastic properties, hardness and fatigue of calcium aluminosilicate glasses in the mid/intermediate silica range," J. Non-Cryst. Solids **434**, 1–12 (2016).
28. M. F. Ando, O. Benzine, Z. Pan, J.-L. Garden, K. Wondraczek, S. Grimm, K. Schuster, and L. Wondraczek, "Boson peak, heterogeneity and intermediate-range order in binary SiO_2-Al_2O_3 glasses," Sci. Rep. **8**(1), 5394 (2018).
29. S. Iftekhar, J. Grins, and M. Eden, "Composition-property relationships of the La_2O_3-Al_2O_3-SiO_2-glass system," J. Non-Cryst. Solids **356**(20-22), 1043–1048 (2010).
30. J. E. Shelby, "Rare Elements in Glasses," Key Eng. Mat., Trans Tech Publications, Switzerland **94-95**, 2–17 (1994).
31. A. Makehima, Y. Tamura, and T. Sakaino, "Elastic moduli and refractive indices of aluminosilicate glasses containing Y_2O_3, La_2O_3, and TiO_2," J. Am. Ceram. Soc. **61**(5-6), 247–249 (1978).
32. L. G. Hwa, T. H. Lee, and S. P. Szu, "Elastic properties of lanthanum aluminosilicate glasses," Mater. Res. Bull. **39**(1), 33–40 (2004).
33. L. Bois, M. J. Guittet, N. Barre, P. Trocellier, S. Guillope, M. Gautier, P. Verdier, and Y. Laurent, "Aqueous alteration of lanthanum alumino-silicate glasses," J. Non-Cryst. Solids **276**(1-3), 181–194 (2000).
34. C. Karras, D. Litzkendorf, S. Grimm, K. Schuster, W. Paa, and H. Stafast, "Nonlinear refractive index study on SiO_2-Al_2O_3- La_2O_3 glasses," Opt. Mater. Express **4**(10), 2066–2077 (2014).
35. K. Schuster, J. Kobelke, D. Litzkendorf, A. Schwuchow, F. Lindner, J. Kirchhof, H. Bartelt, J.-L. Auguste, G. Humbert, and J.-M. Blondy, "Structured material combined HMO-silica fibers: preparation, optical and mechanical behavior," Proc. SPIE **7934**, 79340O (2011).
36. D. Litzkendorf, S. Grimm, K. Schuster, J. Kobelke, A. Schwuchow, A. Ludwig, J. Kirchhof, M. Leich, S. Jetschke, J. Dellith, J.-L. Auguste, and G. Humbert, "Study of lanthanum aluminum silicate glasses for passive and active optical fibers," Int. J. Appl. Glass Sci. **3**(4), 321–331 (2012).
37. P. D. Dragic, C. Kucera, J. Ballato, D. Litzkendorf, J. Dellith, and K. Schuster, "Brillouin scattering properties of lanthano-aluminosilicate optical fiber," Appl. Opt. **53**(25), 5660–5671 (2014).
38. J.-L. Auguste, G. Humbert, S. Leparmentier, M. Kudinova, P.-O. Martin, G. Delaizir, K. Schuster, and D. Litzkendorf, "Modified powder-in-tube technique based on the consolidation processing of powder materials for fabricating specialty optical fibers," Materials **7**(8), 6045–6063 (2014).

Optical Materials EXPRESS

39. K. Schuster, S. Unger, C. Aichele, F. Lindner, S. Grimm, D. Litzkendorf, J. Kobelke, J. Bierlich, K. Wondraczek, and H. Bartelt, "Material and technology trends in fiber optics," Adv. Opt. Technol. **3**(4), 447–468 (2014).
40. M. J. Dejneka, B. Z. Hanson, S. G. Crigler, L. A. Zenteno, J. D. Minelly, D. C. Allan, W. J. Miller, and D. Kuksenkov, "La_2O_3-Al_2O_3-SiO_2 glasses for high-power, Yb3+-doped, 980-nm fiber lasers,"," J. Am. Ceram. Soc. **85**(5), 1100–1106 (2004).
41. M. Loeser, F. Röser, A. Reichelt, M. Siebold, S. Grimm, D. Litzkendorf, A. Schwuchow, J. Kirchhof, and U. Schramm, "Broadband, diode pumped Yb:SiO_2 multicomponent glass laser," Opt. Lett. **37**(19), 4029–4031 (2012).
42. C. Karras, W. Paa, D. Litzkendorf, S. Grimm, K. Schuster, and H. Stafast, "SiO_2-Al_2O_3-La_2O_3 glass - a superior medium for optical Kerr gating at moderate pump intensity," Opt. Mater. Express **6**(1), 125–130 (2016).
43. https://nickelinstitute.org/media/1699/high_temperaturecharacteristicsofstainlesssteel_9004_.pdf.
44. http://www.isolthermics.com.au/metals/pdfs/common-tech/Nicrofer%206023%20-%206023H%20-%20alloy%20601%20-%20601H.pdf.
45. C. J. Voyce, A. D. Fitt, J. R. Hayes, and T. M. Monro, "Mathematical modeling of the self-pressurizing mechanism for microstructured fiber drawing," J. Lightwave Technol. **27**(7), 871–878 (2009).
46. A. N. Denisov, A. F. Kosolapov, A. K. Senatorov, P. E. Pal'tsev, and S. L. Semjonov, "Fabrication of microstructured optical fibers by drawing preforms sealed at their top end," Quantum Electron. **46**(11), 1031–1039 (2016).
47. H. Ebendorff-Heidepriem, "Glasses for infrared fiber applications," in *European Conference on Optical Communication (ECOC) (2013)*, London (UK), 22-26 Sep 2013.
48. R. H. Doremus, "Viscosity of silica," J. Appl. Phys. **92**(12), 7619–7629 (2002).
49. N. Sadiki, J. P. Coutures, C. Fillet, and J. L. Dussossoy, "Crystallization of lanthanum and yttrium aluminosilicate glasses," J. Nucl. Mater. **348**(1-2), 70–78 (2006).
50. F. E. Wagstaff and K. J. Richards, "Kinetics of crystallization of stochiometric SiO_2 glass in H_2O atmospheres," J. Am. Ceram. Soc. **49**(3), 118–121 (1966).
51. F. E. Wagstaff, "Crystallization kinetics of internally nucleated vitreous silica," J. Am. Ceram. Soc. **51**(8), 449–453 (1968).
52. P. P. Bihuniak, "Effect of trace impurities on devitrification of vitreous silica," J. Am. Ceram. Soc. **66**(10), c188–c189 (1983).
53. P. W. France, "*Fluoride Glass Optical Fibres*," (CRC Press. Inc., Springer Netherlands, 1990), 186–204.